Acta Pharmaceutica Sinica B 2025;15(11):5772−5788

Chinese Pharmaceutical Association
Institute of Materia Medica, Chinese Academy of Medical Sciences

Acta Pharmaceutica Sinica B

www.elsevier.com/locate/apsb
www.sciencedirect.com

ORIGINAL ARTICLE

Brain endothelial HIF-1α exacerbates diabetes-associated cognitive impairment by accelerating glycolysis-driven lactate production

Jicong Chen[a], Ruohui Lin[a], Cuihua Jiang[b], Fang Chen[c], Wei Li[d], Lei Wang[a], Ke Pan[a], Jian Zhang[b,*], Zhiqi Yin[a,*], Yaping Huang[a,*]

[a]*School of Traditional Chinese Pharmacy, China Pharmaceutical University, Nanjing 211198, China*
[b]*Affiliated Hospital of Integrated Traditional Chinese and Western Medicine, Nanjing University of Chinese Medicine, Nanjing 210028, China*
[c]*Key Laboratory of Human Functional Genomics of Jiangsu Province, Nanjing Medical University, Nanjing 211166, China*
[d]*Affiliated Jiangning Hospital of Chinese Medicine, China Pharmaceutical University (Nanjing Jiangning Hospital of Chinese Medicine), Nanjing 211100, China*

Received 5 April 2025; received in revised form 28 May 2025; accepted 24 June 2025

KEY WORDS

Type 2 diabetes;
Cognitive impairment;
HIF-1α;
Lactate;
Adult hippocampal neurogenesis;
Brain ECs;
Glycolysis;
Asiatic acid

Abstract Type 2 diabetes (T2D) is an independent risk factor for cognitive impairment. The dysregulation of hypoxia inducible factor (HIF) signaling in T2D patients results in impaired adaptive responses to hypoxia, thereby accelerating the progression of complications. However, limited knowledge is available regarding its precise function in diabetes-associated cognitive impairment (DACI). Here, elevated HIF-1α levels were observed in brain endothelial cells (ECs) of *db*/*db* mice. Functionally, brain ECs-specific knockdown of *Hif1a* significantly ameliorated T2D-induced memory loss and neuronal damage. Glycolysis in brain ECs was inhibited in this process, as indicated by RNA-seq, leading to decreased hippocampal lactate production through reduced LDHA expression. Notably, T2D patients showed increased cerebrospinal fluid lactate levels, which were strongly associated with their cognitive dysfunction. Intrahippocampal injection of lactate accelerated cognitive dysfunction and impaired adult hippocampal neurogenesis (AHN) in *db*/*db* mice. Conversely, reducing hippocampal lactate levels through the intrahippocampal injection of oxamate delayed the onset of memory deficits. Furthermore, asiatic acid was discovered to protect *db*/*db* mice from cognitive impairment by decreasing brain endothelial HIF-

*Corresponding authors.
E-mail addresses: zhangjian@jsatcm.com (Jian Zhang), cpu-yzq@cpu.edu.cn (Zhiqi Yin), yapinghuang@cpu.edu.cn (Yaping Huang).
Peer review under the responsibility of Chinese Pharmaceutical Association and Institute of Materia Medica, Chinese Academy of Medical Sciences.

https://doi.org/10.1016/j.apsb.2025.09.028

1α expression and subsequently reducing hippocampal lactate-induced AHN damage. Overall, this study elucidates the inhibiting role played by endothelial HIF-1α-driven lactate in AHN and highlights a potential tactic of targeting HIF-1α in brain ECs for treating cognitive impairment.

1. Introduction

Type 2 diabetes (T2D), characterized by hyperglycemia, is an independent risk factor for cognitive impairment, including mild cognitive impairment and dementia, which detrimentally affects the capacities of patients in daily activities, occupational performance, and social interactions[1,2]. Given the increasing incidence of T2D and rising life expectancy worldwide[3], effective and feasible intervention strategies are urgently required to prevent the prevalence of diabetes-associated cognitive impairment (DACI). However, clinical trials have shown limited benefits for cognitive function from optimizing glycemic control in T2D patients, such as through regular glucose monitoring and the use of hypoglycemic agents[4]. Hence, it is essential to elucidate the complex mechanisms underlying DACI to propose novel therapeutic avenues.

Hypoxia-inducible factor (HIF) family consists of three members: HIF-1, HIF-2, and HIF-3, which play crucial roles in cellular and systemic adaptation to hypoxia. Structurally, the formation of a dimer between the regulatory α subunit and the constitutively expressed β subunit endows HIFs with the ability to exert biological functions[5−7]. Therefore, the expression level of α subunit of HIFs is the main factor affecting their downstream signaling. Growing evidence has pointed out the dysregulation of HIF signaling in various tissues of T2D patients and animal models, leading to impaired adaptive responses to hypoxia, cellular disorders, and consequently, the complications of T2D[8]. In brain tissue, elevated hippocampal HIF-1α and HIF-2α levels have been reported to evoke the tau and α-synuclein hyperphosphorylation, respectively, and contribute to cognitive dysfunction in chronic hypoxia[9,10]. These studies suggest that HIFs may serve as a potential link between T2D and cognitive impairment[11]. However, the changes of HIF signaling in brain tissues in T2D, particularly at the cellular level, and their underlying mechanisms involving DACI remain elusive and need further investigation.

Adult hippocampal neurogenesis (AHN) is a distinctive form of neuroplasticity characterized by the continuous generation of new neurons from neural stem cells (NSCs) residing in the subgranular zone, which upon maturation are integrated into hippocampal circuits contributing to memory encoding and retrieval[12−14]. AHN persists throughout life in the human brain and is associated with cognition[15]. Patients with diabetes show reduced AHN estimated by atrophy of hippocampus on magnetic resonance imaging[16,17]. Animal models of T2D also exhibit reduced cell proliferation and diminished neuronal differentiation of NSCs, as well as decreased survival of newborn neurons from NSCs in the hippocampus compared to non-diabetic animals[18]. These findings support a notion that T2D contributes to impaired AHN, resulting in DACI. AHN is regulated by multiple intracellular signaling of NSCs and mediators originating from other central or peripheral cells. For instance, Wnt[19], Notch[20], brain-derived neurotrophic factor signaling[21], and some signaling molecules derived from the surrounding cells, such as lactate from endothelial cells (ECs)[14] and chitinase-3-like from astrocytes[22], which exert various effects in hippocampus neurogenesis. Notably, HIFs have been reported to crosstalk with some of the signaling and signal molecules related to AHN mentioned above[23−25], which suggests the potential of HIFs-targeted approaches in promoting AHN and cognitive function. The biological role of HIFs in AHN impaired by T2D, however, is still largely unexplored.

In this study, we noted that elevated brain endothelial HIF-1α levels in the hippocampus under T2D conditions based on analysis of public transcriptomic data and experimental validation. The relationship between endothelial HIF-1α and cognitive function was explored using mice of brain endothelial-specific knockdown of *Hif1a*. Glycolysis-driven lactate was identified as a potential mediator regulated by endothelial HIF-1α in T2D *via* RNA-seq analysis. Subsequently, we investigated the association between elevated lactate levels and cognitive impairment in T2D patients and animals. The role of hippocampal lactate in DACI was determined by either intrahippocampal administration or restriction of lactate in mice. Parallelly, the effect of lactate on AHN was evaluated *in vivo* and *in vitro*. Additionally, natural compounds were screened to inhibit HIF-1α expression in brain ECs and further assessed for the capability to ameliorate impaired AHN and cognitive function in T2D mice.

2. Materials and methods

2.1. Experimental animals

Male *db*/*db* mice (12−20 weeks old) and age-matched *db*/*m* mice were purchased from GemPharmatech (Nanjing, China). All mice were maintained under constant humidity and temperature in the center for experimental animals at China Pharmaceutical University (Nanjing, China) with access to food and water *ad libitum*. All procedures involving animals were performed following protocols approved by the Ethics Committee for animal research of China Pharmaceutical University and conformed to the guidelines for the care and use of laboratory (Approval AEWC-20220913-2).

2.2. Human samples

The clinical study was approved by the Ethics Committee of Fujian Medical University Union Hospital (Approval No. 2020YF004-01), and written informed consent was obtained from all participating individuals. Mini-mental state examination (MMSE) and Montreal cognitive assessment (MoCA) scores were collected from individuals aged over 50 years, both with and without T2D. Meanwhile, lactate levels in the cerebrospinal fluid (CSF) were measured, followed by a correlation analysis between lactate levels and cognitive function score. Above human samples

were donated by Professor Pan Xiaodong from Fujian Medical University Union Hospital (China).

2.3. Data mining of RNA sequencing date

Original data from GSE125387 in GEO database[26], which contains RNA sequencing data of the hippocampal tissue separated from *db*/*m* or *db*/*db* mice, were reanalyzed using DESeq2 R package. The mRNA expressions of *Hif1a*, *Hif2a*, and *Hif3a* were calculated as Transcript by Million (TPM).

2.4. Morris water maze (MWM) test

The experimental procedure was conducted as described previously, including training trials and a probe test[14]. Briefly, from the 1st day to the 5th day, a platform was positioned in a fixed location known as the target quadrant, and all mice were trained once daily. Both escape latency and swimming path were recorded. On the 6th day, the platform was removed, and the time spent in the target quadrant and the number of platform crossings were monitored in 60 s.

2.5. Y maze test

Mice were placed in a fixed arm, and the sequence of mouse entry into different arms was recorded over 5 min, respectively. The spontaneous alternation rate was calculated according to a previous study[27].

2.6. Novel object recognition (NOR) test

All experimental procedure was performed as described previously[14]. Each mouse underwent a habituation phase in an object-free arena for 10 min on the 1st day. On the 2nd day, mice were habituated to the arena for 15 min with two identical objects. After 1 h, one of the familiar objects was replaced with a novel object, and the mice were placed in the arena again for a 10-min exploration session. The exploratory preference was quantified as the percentage of time spent investigating the novel object out of total time spent exploring all objects.

2.7. Data mining of single-cell RNA sequencing date

The hippocampal single-cell RNA-seq data of *db*/*db* and *db*/*m* mice were obtained from GSE201644[28]. The 10 × Genomics raw data were processed using the Seurat package (v5.1.0) to produce a unique molecular identifier (UMI) count matrix. Cells with more than 300 genes and fewer than 7000 genes, more than 400 UMIs, and less than 20% mitochondrial RNA were retained for subsequent analyses. The filtered matrix was normalized and scaled for library size to gain normalized counts. The Uniform Manifold Approximation and Projection method was used to visualize the clustering results for the cells. Cell type annotation was performed using the SingleR (v2.6.0) and celldex (v1.14.0) packages. The "FeaturePlot" function was used to display the expression distribution of genes across various cell types. All analyses were conducted in R (4.4.1).

2.8. Cell culture

Mouse brain-derived endothelial cells.3 (bEnd.3) was obtained from American Type Culture Collection and cultured at 37 °C in an atmosphere of 5% CO_2 in high-glucose Dulbecco's modified Eagle's medium (DMEM, KeyGEN BioTECH, Nanjing, China) supplemented with 10% fetal bovine serum (FBS, KeyGEN BioTECH, Nanjing, China). NSCs were cultured in DMEM/F12 medium (KeyGEN BioTECH, Nanjing, China) supplemented with 1% B-27 supplements (NEST Biotechnology, Wuxi, China), 20 ng/mL epidermal growth factor (PeproTech, NJ, USA), and 20 ng/mL basic fibroblast growth factor (PeproTech, NJ, USA) according to a previously described method[29]. In short, mouse hippocampus was obtained, cut into small pieces, and incubated with 0.125% trypsin solution (KeyGEN BioTECH, Nanjing, China) for 15 min at 37 °C. Gently triturate to prepare a single cell suspension, which was plated into a 24-well plate (NEST Biotechnology, Wuxi, China) and cultured in the proliferation medium. Brain endothelial cells were cultured in the DMEM/F12 medium supplemented with 20% FBS, 2% L-glutamine (MedChemExpress, NJ, USA), and 1 ng/mL basic fibroblast growth factor according to a previously described method[30]. Briefly, mouse hippocampus was obtained, cut into small pieces, and incubated with 2.5% trypsin solution for 20 min at 37 °C. Next, the precipitate was incubated with collagenase type IV (Yeasen, Shanghai, China) for 30 min at 37 °C.

2.9. Cell viability and neurosphere formation assay

In the cell viability tests, NSCs were prepared as a single cell suspension and plated into a 96-well plate (Bioland, Hangzhou, China). Cell viability was evaluated using cell counting kit-8 (APExBIO, Houston, USA). All procedures of the neurosphere formation assay were performed as described previously[29]. NSCs were cultured in the proliferation medium in a 24-well plate (Bioland, Hangzhou, China). Five days later, the number and diameter of neurospheres were calculated after intervention using Image J software.

2.10. Adeno-associated virus (AAV) infection

To knock down the expression of *Hif1a* in brain ECs, AAV2/9-mediated delivery was employed for *db*/*m* or *db*/*db* mice. AAV2/9 encoding mouse *Hif1a* and endothelial cell-specific promoter were provided by Hanheng Biotechnology. In brief, mice were anesthetized with pentobarbital sodium (30 mg/kg, i.p.) and injected with 1.9×10^{12} vector genome/mL HBAAV2/9-tie-mir30-*m*-*Hif1a*-ZsGreen and 1.5×10^{12} vector genome/mL HBAAV2/9-tie-ZsGreen control into hippocampal tissue (5 μL) through microinjector and stereotaxic apparatus.

2.11. Biochemical assay

Glucose levels in serum were tested using blood glucose content assay kits (Solarbio, Beijing, China) following the manufacturer's protocol.

2.12. Enzyme-linked immunosorbent assay (ELISA)

Glycated serum protein (GSP) levels were measured using commercial kits (Jiangsu Meimian Industrial Co., Ltd., Yancheng, China) according to the manufacturer's instructions.

2.13. Nissl staining

Mice were perfused with cold phosphate-buffered saline (PBS, KeyGen, Nanjing, China), and brain tissue was fixed in 4% paraformaldehyde (PFA, KeyGen, Nanjing, China). Next, these tissues were embedded in paraffin, cut into 10 μm thick sections, dewaxed, and stained with cresyl violet acetate. All pictures were captured using an inverted fluorescent microscope (Nikon, Tokyo, Japan).

2.14. RNA sequencing

Total RNA was extracted separately from primary brain ECs isolated from *db*/*db* mice with endothelial *Hif1a* specific knockdown and control using the RNA isolator total RNA extraction reagent (Vazyme, Nanjing, China), separately. EdgeR algorithm was applied to filter differentially expressed genes (DEGs) through $\log FC > 1$ or < -1, and P value < 0.05. Cluster analysis and principal component analysis were performed based on DEGs. Gene Ontology (GO) enrichment analyses were performed using the DAVID database. The fold change of the TPM was analyzed by gene set enrichment analysis (GSEA) with the GO dataset.

2.15. Intrahippocampal injection of lactate and oxamate

The experimental procedure was conducted as described previously[13]. Specifically, mice were anesthetized using pentobarbital sodium (30 mg/kg, i.p.) and subsequently secured in a stereotaxic apparatus. A longitudinal incision was made along the sagittal suture to fully expose the skull surface. Burr holes were then drilled at the following coordinates relative to bregma: anteroposterior, −2 mm; lateral, +1.7 mm; and ventral, −1.9 mm (from dura). Lactate (Sigma, Saint Louis, MO, USA) and oxamate (Sigma) were dissolved in saline at a concentration of 10 mmol/L. The solution was injected into the hippocampus at 2 μL per mouse, with the injection rate carefully maintained at 0.2 μL/min. The needle was left in place for an additional 5 min post-injection.

2.16. Lactate analysis

Hippocampus tissues and cultured cells were homogenized with PBS, followed by centrifugation at 4 °C using 12,000×g for 15 min. The supernatant was collected and protein concentration was determined using the enhanced BCA protein assay kit (Beyotime, Shanghai, China). Additionally, cell culture supernatant was collected and centrifuged at 4 °C using 12,000×g for 15 min. Lactate levels were tested using the lactic acid content assay kit (Solarbio, Beijing, China) following the manufacturer's instructions.

2.17. Advanced glycation end products (AGEs) preparation

AGEs were conducted by co-incubating bovine serum albumin (BSA, Solarbio, Beijing, China) with methylglyoxal (10 mg/mL, Macklin, Shanghai, China) at 37 °C in the dark for 1 week as previously described[31]. Unbound methylglyoxal was subsequently removed through dialysis in PBS for three days.

2.18. Transmission electron microscope (TEM)

The experimental procedure was conducted following previously described methods[32]. Hippocampus tissues were obtained, diced into small blocks, and fixed with 1% osmium tetroxide at room temperature (RT) for 2 h. Subsequently, the tissues were embedded in epon and dissected into ultrathin slices of 70 nm thickness after dehydration and permeation. These slices were then stained with 2% uranyl acetate and lead citrate for 15 min before being examined using a transmission electron microscope (Hitachi, Tokyo, Japan).

2.19. Immunofluorescence staining

Brain tissue sections were fixed within 4% PFA for 30 min, permeabilized with 1% Triton X-100 (Thermo, Waltham, MA, USA) at RT for 30 min, and blocked with 5% BSA at RT for 60 min. Then, samples were incubated with primary antibody at 4 °C in the dark overnight, followed by incubation with fluorescently labeled-secondary antibody at RT for 2 h, counterstained with DAPI to recognize nuclei. All pictures were captured using a microscope (Nikon, Tokyo, Japan).

2.20. Western blot

Proteins were extracted from the collected hippocampus tissues and cells using RIPA lysis buffer supplemented with PMSF on ice, followed by centrifugation at 12,000×g for 10 min at 4 °C. Protein content was determined using the enhanced BCA protein assay kit. Equal protein samples were subjected to SDS-PAGE, transferred onto nitrocellulose membrane, blocked with 5% BSA for 2 h, and incubated with primary antibodies as follows at 4 °C overnight: HIF-1α (Bioss, Beijing, China), HK2 (Abcam, Cambridge, UK), LDHA (Bioss, Beijing, China), Ki67 (Wanleibio, Shenyang, China), PCNA (Wanleibio, Shenyang, China), and β-Tubulin (Proteintech, Wuhan, China), respectively. Next, the membranes were incubated with a horseradish peroxidase-conjugated secondary antibody (Wanleibio, Shenyang, China) and visualized using a commercial enhanced chemiluminescence kit (New Cell & Molecular Biotech, Suzhou, China). Grey values were quantified using Image J software and normalized to expressions of β-Tubulin as internal standard.

2.21. Real-time fluorescence quantitative polymerase chain reaction (RT-qPCR)

Total RNA was extracted from hippocampal tissues or cells using the RNA isolator total RNA extraction reagent (Vazyme, Nanjing, China) and reverse-transcribed by all-in-one first-strand synthesis master mix (Best Enzymes, Lianyungang, China). Taq-HS SYBR green qPCR premix (Best Enzymes) was applied to transcribe the cDNA in a real-time qPCR system. All data were analyzed utilizing the comparative C_T method with *Actb* as the internal standard. Primers were synthesized (Generay Biotech, Shanghai, China) using the sequences shown in Supporting Information Table S1.

2.22. Statistical analysis

The Kolmogorov−Smirnov test was used to assess the normality of the data. For data with normal distributions, one-way ANOVA with Tukey's *post hoc* test was utilized to evaluate differences among more than two groups and adjust for multiple comparisons; otherwise, the Kruskal−Wallis test was applied. To compare differences between two groups, Student's t-test was used for pairwise comparisons assuming normal distribution; otherwise, the

Mann−Whitney *U* test was performed. Correlations between two parameters were assessed using Pearson's correlation coefficient. The data are presented as mean ± standard error of mean (SEM), and a P value < 0.05 was considered statistically significant.

3. Results

3.1. Elevated hippocampal HIF-1α level is associated with cognitive impairment in db/db mice

The RNA-seq data (GSE125387) of mouse hippocampal tissue with and without T2D were reanalyzed to investigate the potential mechanisms underlying DACI. As shown in Fig. 1A, the mRNA levels of *Hif1a* and *Hif3a* but not *Hif2a* were significantly increased in the hippocampal tissues of *db*/*db* mice ($n = 10$), which exhibited increased glucose levels, reduced insulin levels, and elevated AGEs levels (Supporting Information Fig. S1A), compared with controls ($n = 11$). HIF-1α was assessed *in vivo* due to its abundant expression (Fig. 1B). Western blot analysis revealed that hippocampal HIF-1α protein expression was significantly upregulated in *db*/*db* mice compared with *db*/*m* mice (Fig. 1C and D). Similarly, a remarkable elevation of hippocampal *Hif1a* mRNA level was observed in *db*/*db* mice compared with controls (Fig. 1E). Immunofluorescence staining results confirmed an increased fluorescence intensity of HIF-1α^+ area in the hippocampus of *db*/*db* mice (Fig. 1F, Fig. S1B). The learning and memory abilities of *db*/*db* ($n = 29$) and *db*/*m* ($n = 18$) mice were evaluated through behavior experiments. In the training trial of MWM, the escape latency of *db*/*db* mice was remarkably longer compared to controls, suggesting a decline in learning capacity (Fig. 1G and H). During the probe trial, *db*/*db* mice exhibited a reduced number of platform crossings than *db*/*m* mice, while no significant change was observed in the target-zone duration, which indicated a slight deficit in spatial memory (Fig. 1I and J). In the Y maze test, there was a significant decrease in spontaneous alternation rate shown by *db*/*db* mice compared to controls (Fig. 1K, Fig. S1C). Additionally, *db*/*db* mice exhibited decreased percentage of exploratory preference compared with *db*/*m* mice in the NOR test (Fig. S1D). In

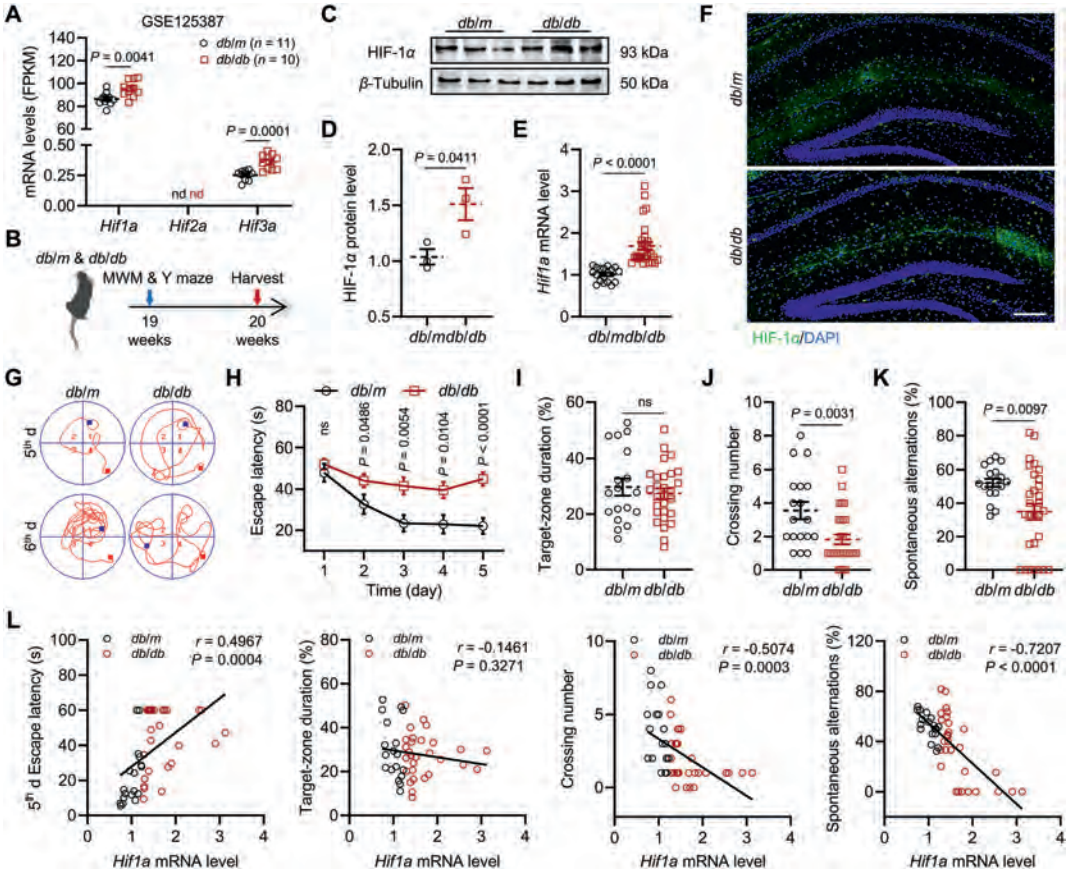

Figure 1 Elevated hippocampal HIF-1α level is associated with cognitive impairment in *db*/*db* mice. (A) The mRNA levels of *Hif1a*, *Hif2a*, and *Hif3a* of mouse hippocampal tissue with and without T2D. Original data was obtained from GSE125387. (B) Experiment outline. Behavioral tests, including MWM and Y maze test, were performed in *db*/*db* mice (19-week-old) and age-matched *db*/*m* mice ($n = 18$ for *db*/*m* mice, $n = 29$ for *db*/*db* mice) to detect the cognitive function. (C, D) Hippocampal HIF-1α expression of *db*/*m* and *db*/*db* mice was assessed using Western blot analysis ($n = 3$ per group). (E) The mRNA levels of *Hif1a* in hippocampus of *db*/*m* and *db*/*db* mice were evaluated by RT-qPCR (normalized to *Actb*; $n = 18$ for *db*/*m* mice, $n = 29$ for *db*/*db* mice). (F) Representative images of HIF-1α^+ areas in hippocampus were assessed by immunofluorescence staining ($n = 3$ per group). Scale bar, 200 μm. (G) Typical swimming paths of 5th and 6th day in MWM test. (H) Escape latency during the training trial of MWM test. (I) Percentage of target-zone duration in MWM test. (J) Number of target-platform crossings in MWM test. (K) Spontaneous alternation rate in Y maze test. (L) Correlation analysis of hippocampal *Hif1a* mRNA level with 5th day escape latency, target-zone duration, target-platform crossing, and spontaneous alternations (r values were calculated by Pearson's method). Data are presented as mean ± SEM. ns, no statistical difference. P values were determined by two-tailed Student's t test or Mann−Whitney U test.

Fig. 1L, a positive correlation was analyzed between hippocampal *Hif1a* mRNA levels and escape latency on the 5th day. Additionally, a negative correlation was observed between hippocampal *Hif1a* mRNA levels and the number of platform crossings as well as the spontaneous alternations rate. In conclusion, these findings demonstrate that elevated hippocampal HIF-1α level was associated with cognitive impairment in *db/db* mice.

3.2. *Knockdown of HIF-1α in brain ECs prevents cognitive impairment in db/db mice*

The single-cell RNA-seq data (GSE201644) were reanalyzed to clarify HIF-1α expression in distinct cell populations within the hippocampus (Supporting Information Fig. S2A−S2C). As shown in Fig. 2A, there was a significant increase in the average

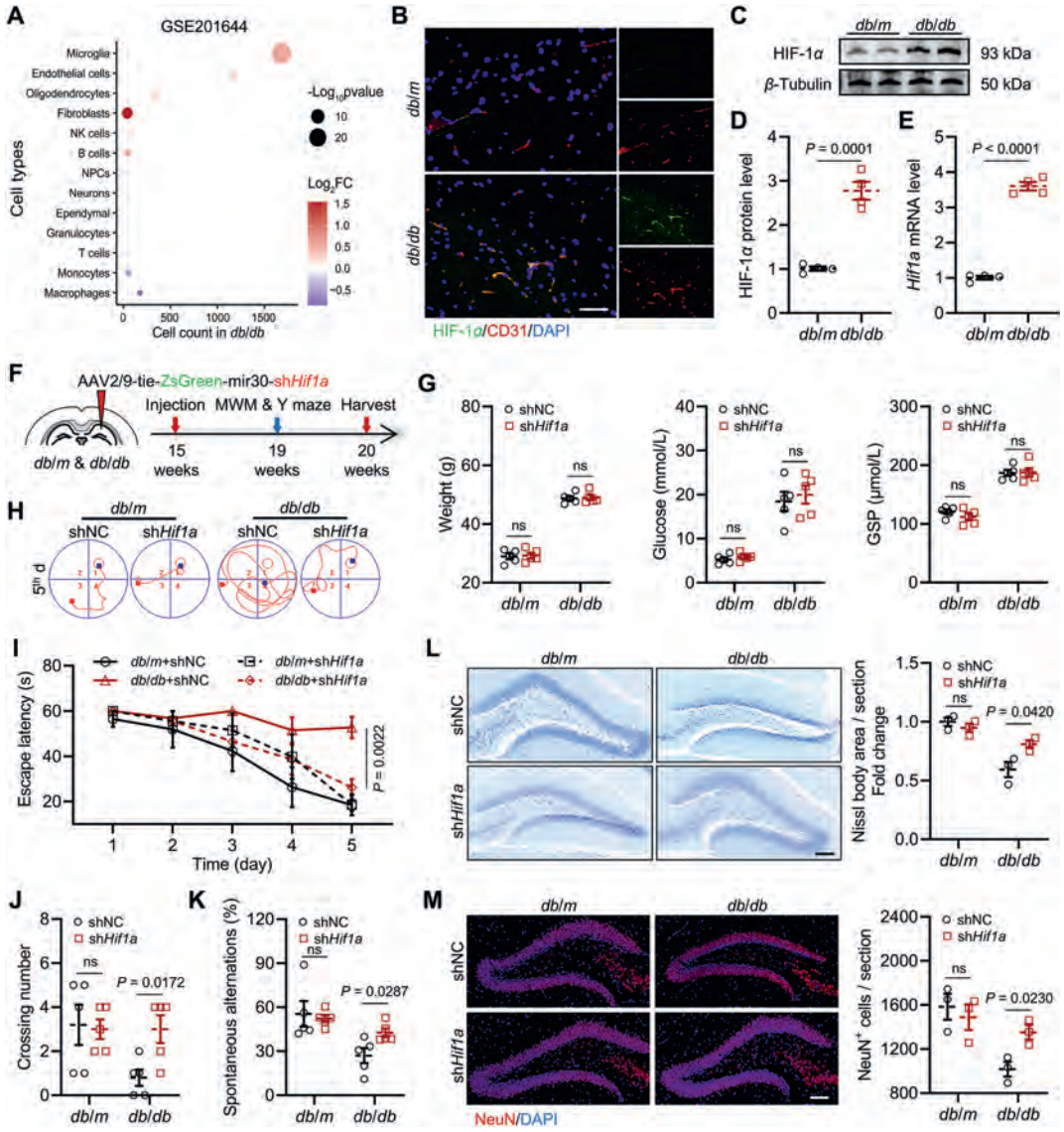

Figure 2 Knockdown of *HIF-1α* in brain ECs prevents cognitive impairment in *db/db* mice. (A) The average expression of *Hif1a* in distinct cell populations within the hippocampus from *db/m* and *db/db* mice. Original data was obtained from GSE201644. (B) Representative images of HIF-1α^+/CD31$^+$ areas in hippocampus of *db/m* and *db/db* mice were assessed by immunofluorescence staining ($n = 3$ per group). Scale bar, 50 μm. (C, D) Representative images and quantification of HIF-1α expression in primary brain ECs isolated from *db/m* and *db/db* mice were assessed through Western blot ($n = 4$ per group). (E) The mRNA levels of *Hif1a* in primary brain ECs isolated from *db/m* and *db/db* mice were evaluated by RT-qPCR (normalized to *Actb*, $n = 4$ per group). (F) Experiment outline. AAV-sh*Hif1a* and AAV-shNC were injected into the hippocampus of 15-week-old mice. Morris water maze (MWM) and Y maze test were performed in *db/db* mice (19-week-old) and age-matched *db/m* mice ($n = 5$ per group) to detect cognitive function. (G) Body weight, serum glucose, and glycosylated serum protein (GSP) of mice at 20 weeks old. (H) Typical swimming paths of 5th day in the MWM test. (I) Escape latency during the training trial of MWM test. (J) Number of target-platform crossings in the MWM test. (K) Spontaneous alternation rate in Y maze test. (L) Representative images and quantification of Nissl staining in DG area of mice ($n = 3$ per group). Scale bar, 50 μm. (M) Representative images and quantification of NeuN$^+$ cells in DG area of mice ($n = 3$ per group) tested by immunofluorescence staining. Scale bar, 50 μm. Data are presented as mean ± SEM. ns, no statistical difference. *P* values were determined by two-tailed Student's *t* test.

expression of *Hif1a* observed in brain ECs from *db*/*db* mice compared to *db*/*m* mice. Immunofluorescence co-localization results further confirmed an increased fluorescence intensity of HIF-1α^{+}/CD31^{+} area in the hippocampus of *db*/*db* mice (Fig. 2B). Consistently, Western blot analysis demonstrated a remarkable upregulation of HIF-1α protein expression in the primary brain ECs isolated from *db*/*db* mice, accompanied by an elevation in *Hif1a* mRNA levels as well (Fig. 2C−E). Briefly, our findings suggested HIF-1α was significantly increased in the brain ECs of *db*/*db* mice.

Next, adeno-associated virus 2/9 encoding *Hif1a* (AAV-*Hif1a*) and AAV-NC were injected into the hippocampus to knock down *Hif1a* expression in the brain ECs. The viral vectors were equipped with an endothelial cell-specific promoter for precise targeting (Fig. 2F). As expected, immunofluorescence staining results demonstrated a significant reduction in HIF-1α expression specifically within brain ECs after 4 weeks (Fig. S2D). No remarkable differences of HIF-1α expression were observed between AAV-NC and AAV-*Hif1a* groups in the heart, liver, spleen, lung, and kidney, as demonstrated by immunohistochemistry assays (Fig. S2E). Western blot analysis revealed that AAV-*Hif1a* injection reduced HIF-1α protein expression in the hippocampus but not in the cortex or hypothalamus (Fig. S2F). Additionally, brain ECs-specific knockdown of *Hif1a* did not affect the body weight, serum glucose, and serum GSP of mice (Fig. 2G). During the navigation trial of MWM, the escape latency of *db*/*db* mice was significantly shorter after brain ECs-specific knockdown of *Hif1a* (Fig. 2H and I). In the probe test, *db*/*db*-sh*Hif1a* mice passed through the original platform location more times than *db*/*db*-shNC mice (Fig. 2J). Consistently, brain ECs-specific knockdown of *Hif1a* rescued the decrease of the spontaneous alternation rate of *db*/*db* mice (Fig. 2K). In Fig. 2L, Nissl staining results showed a significant increase of the area occupied by Nissl bodies within the dentate gyrus (DG) of *db*/*db*-sh*Hif1a* mice compared to *db*/*db*-shNC mice. Moreover, an elevated number of NeuN-positive cells was observed in the DG of *db*/*db* mice after *Hif1a*-specific knockout through immunofluorescence analysis (Fig. 2M). Overall, our data indicated that brain ECs-specific knockdown of *Hif1a* significantly ameliorated memory loss and neuronal damage in *db*/*db* mice.

3.3. Knockdown of HIF-1α inhibits glycolysis-driven lactate production through decreasing LDHA expression

To investigate the potential functional significance of brain endothelial HIF-1α in DACI, RNA-seq was performed to identify the downstream targets regulated by HIF-1α in primary brain ECs isolated from *db*/*db*-shNC and *db*/*db*-sh*Hif1a* mice. In Fig. 3A, DEGs were enriched in the gene sets related to glycolysis, such as "Glycolytic process", "Canonical glycolysis", and "Fructose metabolic process". Among them, "glycolytic process" was significantly inhibited as indicated by GSEA after knockdown of *HIF-1α* (Fig. 3B), with 8 downregulated genes involved in it exhibited in the heat map (Fig. 3C). Consistently, RT-qPCR results further confirmed knockdown of *HIF-1α* inhibited the levels of glycolysis-related genes such as *Ldha* and *Hk2* (Fig. 3D). Western blot analysis revealed upregulation of LDHA and HK2 protein expression in the primary brain ECs isolated from *db*/*db*-shNC mice; however, these expressions were significantly downregulated by *Hif1a* knockdown (Fig. 3E). Lactate, an end-product of glycolysis, plays a multifaceted role as an energy substrate and signal regulatory molecule, which has been increasingly elucidated[33]. As shown in Fig. 3F, significant increases were observed both in the primary brain ECs isolated from *db*/*db*-shNC mice and their supernatant; however, knockdown of *Hif1a* inhibited these increases. Hippocampal lactate levels of *db*/*db* mice were also significantly decreased after brain ECs-specific knockdown of *Hif1a* (Fig. 3G). To further confirm knockdown of *Hif1a* causes the changes of glycolysis-driven lactate production, AGEs and high glucose (HG) were added to bEnd.3 cells to induce upregulation of HIF-1α expression and glycolysis level (Supporting Information Table S2, Fig. S3A−S3F). As expected, knockdown of *Hif1a* decreased the elevated protein expression of LDHA in bEnd.3 cells induced by AGEs (Fig. 3H). Additionally, lactate levels were increased in AGEs-induced and HG-induced bEnd.3 cells and their supernatant; however, knockdown of *Hif1a* inhibited these changes, which exhibited decreased lactate levels (Fig. 3I and Fig. S3G). Subsequently, overexpression of LDHA in AGEs-induced bEnd.3 cells following the knockdown of *Hif1a* led to a significant increase in lactate levels, which approached those induced by AGEs (Fig. 3J and K). In summary, these findings indicated knockdown of *Hif1a* in the brain ECs inhibited glycolysis-driven lactate production through decreasing LDHA expression.

3.4. Elevated hippocampal lactate is associated with impaired cognitive function and AHN in T2D

To explore the underlying impact of brain endothelial HIF-1α-driven lactate in DACI, CSF samples and cognitive scores were collected from non-T2D individuals ($n = 10$) and T2D patients ($n = 21$). As depicted in Fig. 4A, T2D patients exhibited lower scores on MMSE and MoCA, indicating impaired cognitive function in T2D patients. Notably, CSF lactate levels were significantly elevated in T2D patients compared to controls (Fig. 4B). Subsequent analysis revealed an inverse relationship between CSF lactate levels and MMSE as well as MoCA scores (Fig. 4C). In Fig. 4D, *db*/*db* mice exhibited a significant increase in hippocampal lactate level compared to *db*/*m* mice. Consistently, correlation analysis results revealed a positive correlation between hippocampal lactate levels and escape latency on the 5th day, while a negative correlation was observed with the number of platform crossings and spontaneous alternation rate in mice (Fig. 4E). In short, the above findings indicated that elevated hippocampal lactate level is associated with cognitive dysfunction in T2D.

Next, 20-week-old *db*/*db* mice were divided into high-lactate and low-lactate groups based on median hippocampal lactate concentration (0.6763 mmol/gprot, $n = 10$ per group), referring to a previous study (Fig. 4F)[34]. Reanalysis of behavioral data showed a significant decrease in the crossing number and spontaneous alternation rate of *db*/*db* mice in the high-lactate group compared with those in the low-lactate group (Fig. 4G and H). TEM analysis revealed a reduced number of synapses and synaptic vesicles in CA3 of *db*/*db* mice belonging to the high-lactate group (Fig. 4I and J). As evidenced by Nissl staining, a significant reduction in the quantity of Nissl bodies within DG of the high-lactate group compared to the low-lactate group (Fig. 4K). Similarly, there was a notable reduction in NeuN-positive cells within DG among mice from the high-lactate group (Fig. 4L). Given the demonstrated

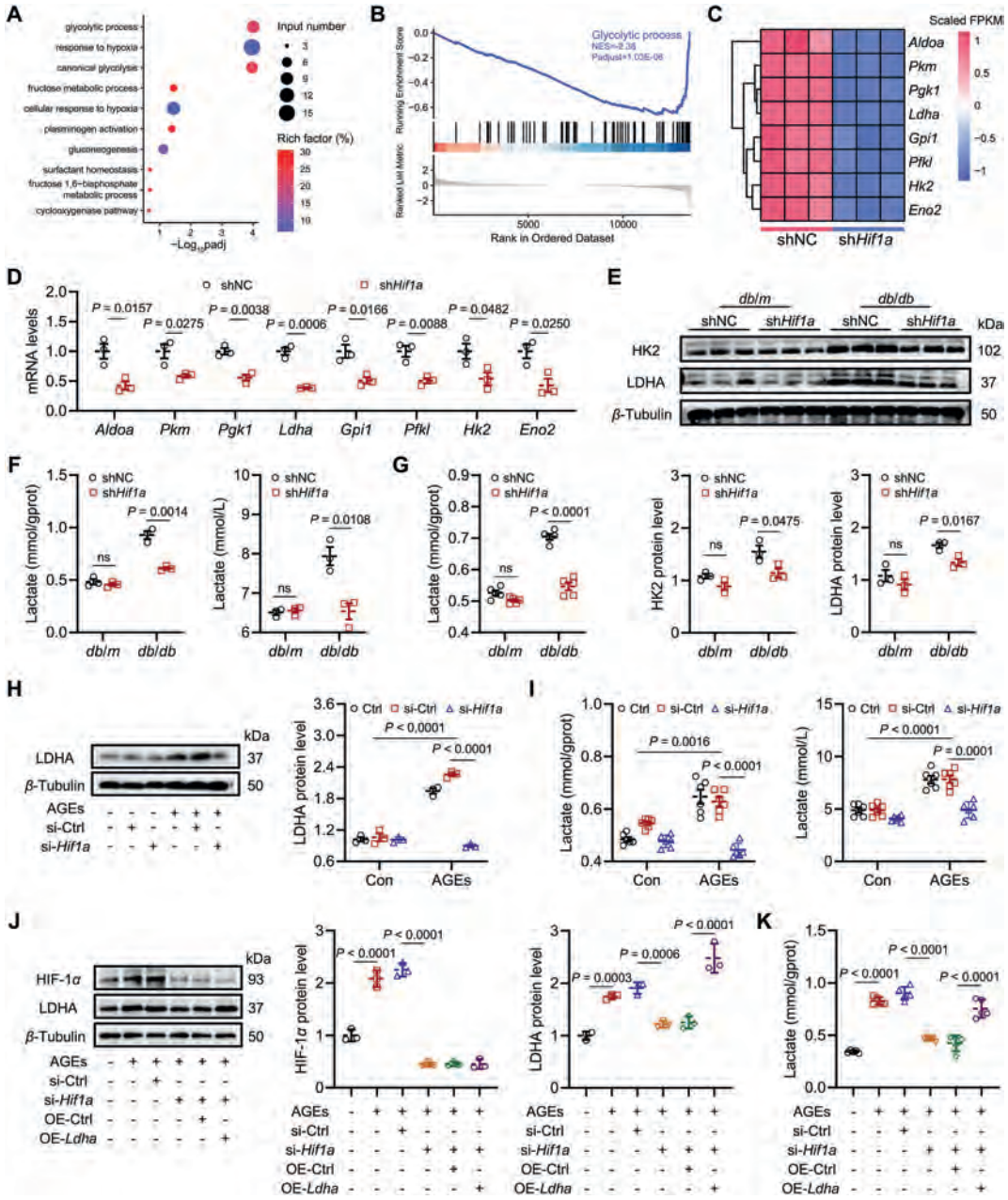

Figure 3 Knockdown of *HIF-1α* inhibits glycolysis-driven lactate production. RNA-Seq was performed in primary brain ECs isolated from *db*/*db*-shNC and *db*/*db*-sh*Hif1a* mice ($n = 3$ per group). (A) Biological process of gene ontology enrichment analysis. (B) Gene set enrichment analysis on glycolytic process. (C) Differentially expressed genes between primary brain ECs isolated from *db*/*db*-shNC and *db*/*db*-sh*Hif1a* mice. (D) The mRNA levels of glycolytic process-related genes tested using RT-qPCR (normalized to *Actb*, $n = 3$ per group). (E) HK2 and LDHA protein expression in primary brain ECs was evaluated by Western blot ($n = 3$ per group). (F) Lactate levels in primary brain ECs and their supernatants were tested using commercial kits ($n = 3$ per group). (G) Hippocampal lactate levels of shNC and sh*Hif1a* mice were assessed using commercial kits ($n = 5$ per group). (H) The LDHA expression of AGEs-induced bEnd.3 cells following *Hif1a* knockdown were evaluated through Western blot ($n = 3$ per group). (I) Lactate levels in AGEs-induced bEnd.3 cells and their supernatants upon *Hif1a* knockdown were measured using commercial kits ($n = 6$ per group). (J) Overexpression and knockdown validation. The expression of HIF-1α and LDHA in AGEs-induced bEnd.3 cells after *Ldh*a overexpression or *Hif1a* knockdown were tested through Western blot ($n = 3$ per group). (K) Lactate levels in AGEs-induced bEnd.3 cells after *Ldh*a overexpression or *Hif1a* knockdown were assessed using commercial kits ($n = 5$ per group). Data are presented as mean ± SEM. ns, no statistical difference. *P* values were determined by two-tailed Student's *t* test or one-way ANOVA, followed by Turkey's test.

direct impact of increased hippocampal lactate on AHN[14], 5-ethynyl-2-deoxyuridine (EdU) was used for labeling all newly generated cells. Both the number of newborn cells (Fig. 4M) and newborn NSCs (Fig. 4N) exhibited significant reduction in DG of mice from the high-lactate group compared to those from the low-lactate group. In short, these findings suggested hippocampal lactate accumulation is associated with impaired AHN under T2D conditions.

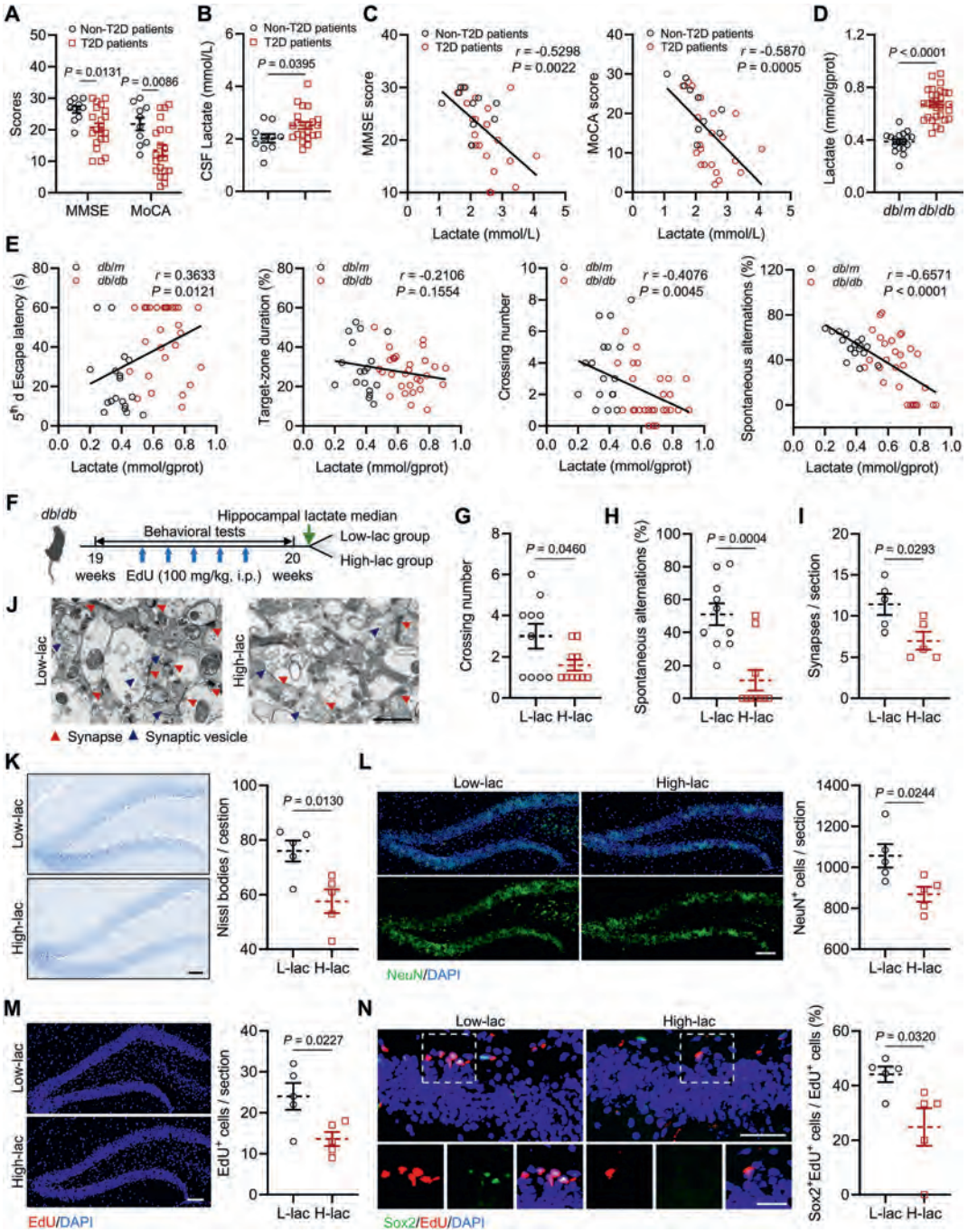

Figure 4 Elevated hippocampal lactate is associated with impaired cognitive function and AHN in T2D. (A) Cognitive scores of non-T2D individuals and T2D patients were assessed through MMSE and MoCA test ($n = 10$ for non-T2D individuals, $n = 21$ for T2D patients). (B) CSF lactate levels of non-T2D individuals and T2D patients were tested using commercial kits. (C) Correlation analysis of CSF lactate levels with MMSE scores and MoCA scores. (D) Hippocampal lactate levels of 20-week-old mice were measured using commercial kits ($n = 18$ for *db*/*m* mice, $n = 29$ for *db*/*db* mice). (E) Correlation analysis of hippocampal lactate levels with 5th day escape latency, target-zone duration, target-platform crossing, and spontaneous alternations. (F) Experiment outline. During behavioral tests, EdU (100 mg/kg) was injected intraperitoneally into *db*/*db* mice five times. Next, all *db*/*db* mice were divided into high-lactate and low-lactate groups based on median lactate concentration (0.6763 mmol/gprot, $n = 10$ per group). (G) Number of target-platform crossings in MWM test. (H) Spontaneous alternation rate in Y maze test. (I, J) Synaptic morphology in CA3 tested by TEM. Scale bar, 1 μm. Quantification of numbers of synapses in (J) ($n = 5$ per group). (K) Representative images and quantification of Nissl staining in DG ($n = 5$ per group). Scale bar, 50 μm. (L) Iconic images and quantification of $NeuN^+$ cells in DG ($n = 5$ per group) tested by immunofluorescence staining. Scale bar, 50 μm. (M) Representative images of EdU^+ cells and quantification in DG ($n = 5$ per group) tested by immunofluorescence staining. Scale bar, 100 μm. (N) Characteristic images of EdU^+ $Sox2^+$ cells and quantification of percentage of $Sox2^+EdU^+/EdU^+$ cells ($n = 5$ per group). Scale bar, 50 μm. Data are presented as mean ± SEM. Correlation coefficient r values were calculated by Pearson's method. P values were determined by two-tailed Student's t test or Mann−Whitney U test.

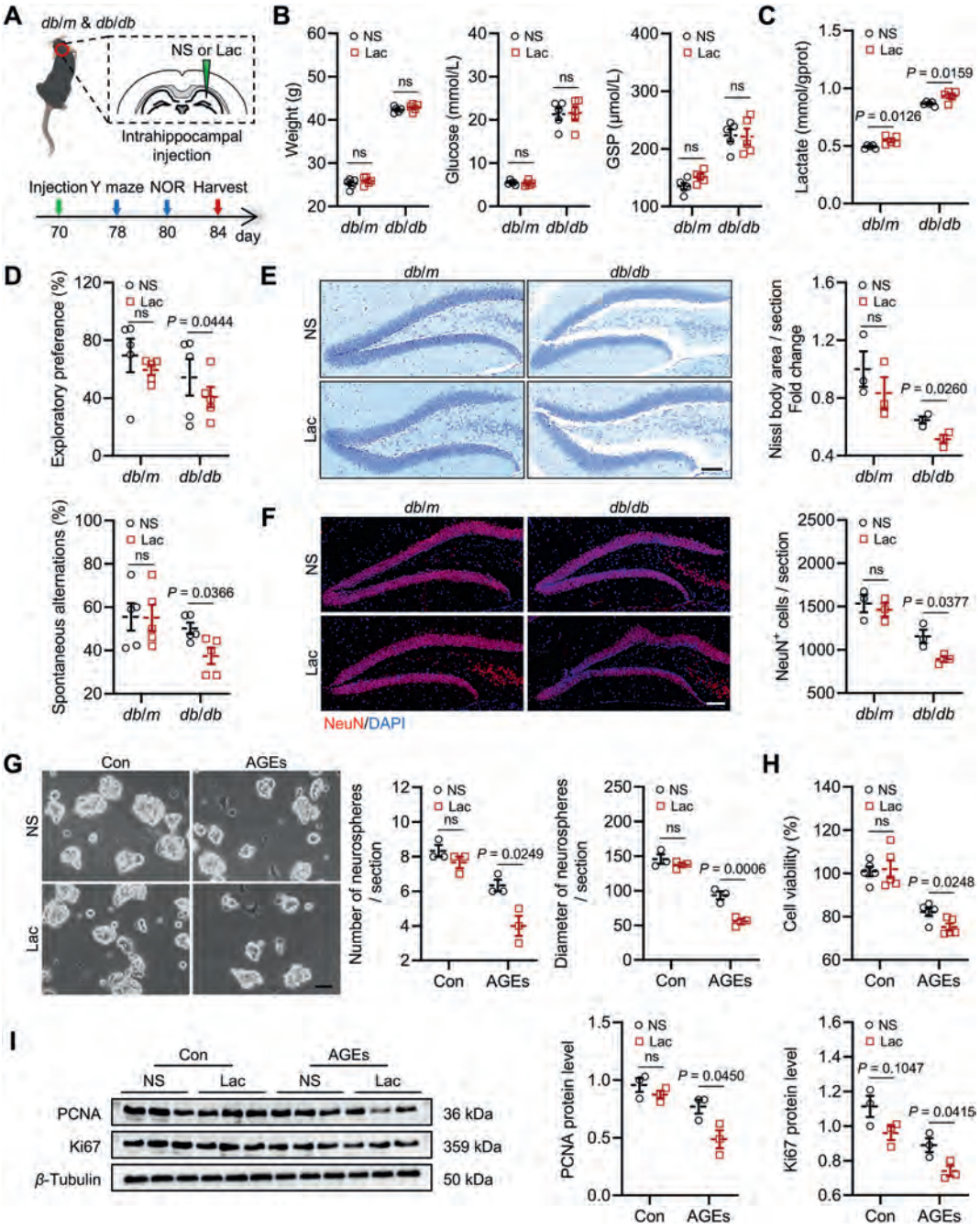

Figure 5 Hippocampal lactate accumulation accelerates T2D-associated cognitive impairment. (A) Experiment outline. Unilateral injections of either saline or 10 mmol/L lactate were administered into the hippocampus of 10-week-old mice ($n = 5$ per group). One week later, behavioral tests including Y maze test and novel object recognition (NOR) test were performed to assess the cognitive ability of mice. (B) Body weight, serum glucose, and glycosylated serum protein were assessed using commercial kits. (C) Hippocampal lactate levels of mice in each group were tested by commercial kits. (D) Spontaneous alternation rate in Y maze test and exploratory preference rate in NOR test. (E) Representative images and quantification of Nissl staining in DG area ($n = 3$ per group). Scale bar, 50 μm. (F) Representative images and quantification of $NeuN^+$ cells in DG area ($n = 3$ per group) were tested by immunofluorescence staining. Scale bar, 50 μm. (G) Representative images and quantification of neurospheres treated with lactate or without lactate. Scale bar, 50 μm. (H) Cell viability of NSCs in each group was tested using CCK-8 kit ($n = 5$ per group). (I) Proliferation-associated proteins (Ki67 and PCNA) levels of NSCs were assessed using Western blot ($n = 3$ per group). Data are presented as mean ± SEM. ns, no statistical difference. *P* values were determined by two-tailed Student's *t* test.

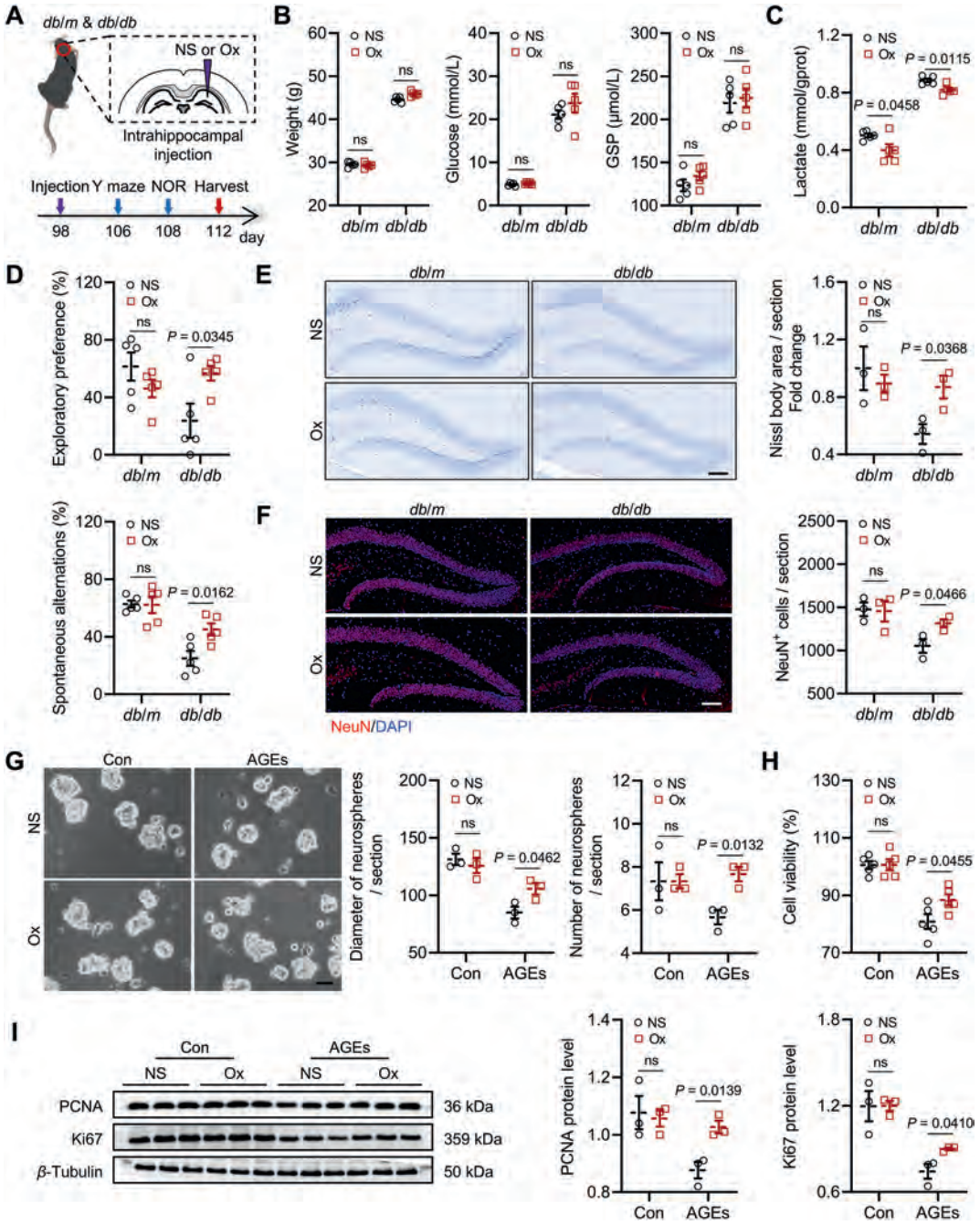

Figure 6 Reducing hippocampal lactate production mitigates T2D-associated cognitive dysfunction. (A) Experiment outline. Unilateral injections of either saline or 10 mmol/L oxamate were administered into the hippocampus of 14-week-old mice ($n = 5$ per group). One week later, behavioral tests including Y maze test and novel object recognition (NOR) test were performed to assess the cognitive ability of mice. (B) Body weight, serum glucose, and glycosylated serum protein were assessed using commercial kits. (C) Hippocampal lactate levels of mice in each group were tested by commercial kits. (D) Spontaneous alternation rate in Y maze test and exploratory preference rate in NOR test. (E) Representative images and quantification of Nissl staining in DG area ($n = 3$ per group). Scale bar, 50 μm. (F) Representative images and quantification of $NeuN^+$ cells in DG area ($n = 3$ per group) were tested by immunofluorescence staining. Scale bar, 50 μm. (G) Representative images and quantification of neurospheres treated with or without Ox. Scale bar, 50 μm. (H) Cell viability of NSCs in each group was tested using CCK-8 kit ($n = 5$ per group). (I) Proliferation-associated proteins (Ki67 and PCNA) levels of NSCs were assessed using Western blot ($n = 3$ per group). Data are presented as mean ± SEM. ns, no statistical difference. *P* values were determined by two-tailed Student's *t* test.

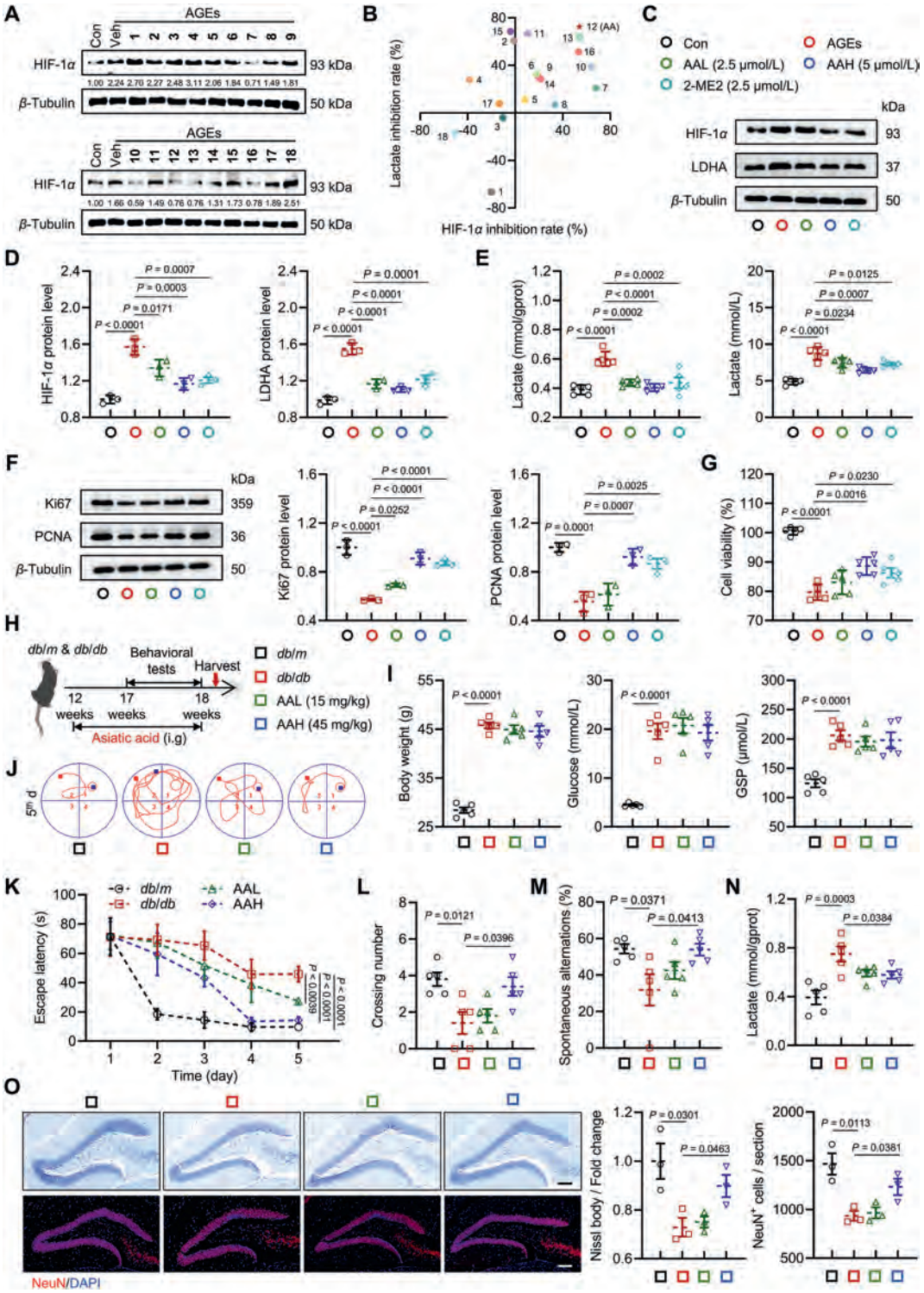

Figure 7 Targeted inhibition of Hif-1α expression in brain ECs by asiatic acid alleviates DACI. (A) HIF-1α expression of AGEs-induced bEnd.3 cells treated with compounds **1**−**18** were tested using Western blot ($n = 3$ per group). (B) Screening candidate compounds by HIF-1α inhibition rate and lactate inhibition rate. (C) HIF-1α and LDHA protein expression of AGEs-induced bEnd.3 cells treated with asiatic acid (AA) or 2-ME2 were assessed through Western blot ($n = 3$ per group). (D) Quantification of HIF-1α and LDHA protein expression in (C). (E) Intracellular and extracellular lactate levels of AGEs-induced bEnd.3 cells treated with or without AA and 2-ME2 were evaluated by commercial kits ($n = 5$ per group). (F) Proliferation-associated proteins (Ki67 and PCNA) levels of NSCs were assessed using Western blot ($n = 3$ per group). (G) Cell viability of NSCs in each group was tested using CCK-8 kit ($n = 5$ per group). (H) Experiment outline. *db*/*db* mice were treated with AA (15, 45 mg/kg) for 6 weeks. MWM and Y maze test were performed ($n = 5$ per group). (I) Body weight, serum glucose, and glycosylated serum protein of each mouse were assessed using commercial kits. (J) Typical 5th day swimming paths in the MWM test. (K) Escape latency during the training trial of MWM. (L) Number of target-platform crossings in the MWM. (M) Spontaneous alternation rate in Y maze test.

3.5. Hippocampal lactate accumulation accelerates T2D-associated cognitive impairment

Unilateral injections of either saline or 10 mmol/L lactate were administered into the hippocampus of 10-week-old mice to assess the impact of elevated lactate levels on cognitive function (Fig. 5A)[14]. No notable difference in body weight, serum glucose, and serum GSP level was observed between mice injected with saline or lactate (Fig. 5B). Compared to control mice treated with saline, injection of lactate significantly increased lactate levels in the hippocampus (Fig. 5C). In behavioral tests, no significant differences were observed among *db*/*m* mice, whereas *db*/*db* mice exhibited diminished spontaneous alternation rate and exploration preferences subsequent to lactate injection (Fig. 5D). As evidenced by Nissl staining, a reduction in the area occupied by Nissl bodies within DG of *db*/*db* mice after lactate injection (Fig. 5E). Similarly, immunofluorescence staining demonstrated a notable decrease in NeuN-positive cell count within DG of *db*/*db* mice after lactate injection (Fig. 5F). Next, NSCs isolated from newborn mice as described in our previous studies[29], which were exposed to AGEs (200 μg/mL) and treated with or without lactate (5 mmol/L). Morphological analysis revealed a decreasing trend in both number and diameter of neurospheres in the AGEs-Lac group compared to the AGEs-NC group (Fig. 5G). In Fig. 5H, a similar decrease of cell viability was observed in the AGEs-Lac group. Additionally, Western blot analysis indicated a significant decrease in the expression levels of proliferation-related proteins (Ki67 and PCNA) following treatment with lactate (Fig. 5I). In short, these data suggested hippocampal lactate accumulation accelerated cognitive impairment in T2D by impairing AHN.

3.6. Reducing hippocampal lactate production mitigates T2D-associated cognitive dysfunction

To further evaluate the negative impact of hippocampal lactate accumulation on cognitive function, we unilaterally injected either saline or oxamate into the hippocampus of 14-week-old *db*/*db* and *db*/*m* mice (Fig. 6A). Oxamate has gained recognition as an LDHA inhibitor and is widely used to reduce lactate production[35]. Injection of oxamate did not affect the body weight, serum glucose, and serum GSP levels compared to control mice injected with saline (Fig. 6B). However, both *db*/*db* and *db*/*m* mice exhibited a remarkable decrease in hippocampal lactate levels following oxamate injection (Fig. 6C). Encouragingly, after receiving intrahippocampal injections of oxamate, *db*/*db* mice showed some improvement in cognitive dysfunction, as evidenced by elevated spontaneous alternation rate and exploration preference (Fig. 6D). Nissl staining revealed a significant increase in the area occupied by Nissl bodies within DG of *db*/*db*-Ox group compared to that observed in the *db*/*db*-NS group (Fig. 6E). Similarly, there was a remarkable increase in the number of NeuN-positive cells within DG after oxamate injection (Fig. 6F). *In vitro*, bEnd.3 cells treated with saline or oxamate (20 mmol/L) were co-cultured with NSCs in a Transwell system, respectively. As evidenced by morphological analysis, NSCs in AGEs-Ox group exhibited larger diameter and greater quantity compared to AGEs-NS group (Fig. 6G). Meanwhile, a significant increase in cell viability and expression levels of proliferation-related proteins (Ki67 and PCNA) was observed in the AGEs-Ox group (Fig. 6H and I). Altogether, inhibition of excessive hippocampal lactate production effectively mitigated cognitive impairment and restored AHN in *db*/*db* mice.

3.7. Targeted inhibition of HIF-1α expression in brain ECs by asiatic acid alleviates T2D-associated cognitive dysfunction

To identify potential compounds targeting HIF-1α, Western blot analysis was applied to evaluate the inhibitory effects of 18 natural compounds isolated from *Cyclocarya paliurus* (Batal.) Iljinsk (Fig. 7A and Supporting Information Table S3). Among them, compound **12** (asiatic acid, AA) was further investigated for exhibiting excellent HIF-1α and lactate inhibitory activities (Fig. 7B). *In vitro*, AA (2.5, 5 μmol/L) effectively mitigated the AGEs-induced upregulation of HIF-1α and LDHA protein expression (Fig. 7C and D). In Fig. 7E, lactate levels in AGEs-induced bEnd.3 cells and their culture supernatant were significantly decreased after AA treatment. NSCs were also co-cultured with bEnd.3 cells, which were treated with AA or 2-methoxyestradiol (2-ME2, 2.5 μmol/L). AA treatment significantly increased both cell viability and the expression of proliferation-related proteins (Ki67 and PCNA) of NSCs, with effects comparable to those observed with 2-ME2 treatment (Fig. 7F and G). Next, *db*/*db* mice were administered with or without AA (15 and 45 mg/kg) for 6 weeks, while age-matched *db*/*m* mice served as the control group (Fig. 7H). There was no remarkable difference in body weight, serum glucose, and serum GSP levels between *db*/*db* mice treated with or without AA (Fig. 7I). In the MWM test, *db*/*db* mice in the AAH group exhibited a significantly reduced swimming path length, decreased escape latency, and an increased number of crossings compared to *db*/*db* mice (Fig. 7J−L). AAH also significantly improved the spontaneous alternation rate of *db*/*db* mice in the Y maze test (Fig. 7M). Additionally, a decrease of hippocampal lactate level in *db*/*db* mice was observed after AA treatment (Fig. 7N). Nissl staining revealed a significant increase in the area occupied by Nissl bodies within DG of AAH group compared to that observed in the *db*/*db* group. Similarly, there was a remarkable increase in the number of NeuN-positive cells within DG after AA treatment (Fig. 7O). Furthermore, the intracerebral distribution of AAH (45 mg/kg) following oral administration was examined to assess its ability to traverse the blood−brain barrier (BBB). LC−MS analysis revealed that the concentration of AA in the brain of both *db*/*m* and *db*/*db* mice was lower than the limit of detection (Supporting Information Fig. S4). In short, these findings suggested AA alleviated T2D-associated cognitive dysfunction through inhibiting HIF-1α expression in brain ECs.

4. Discussion

To date, T2D contributes to the progression of cognitive impairment (Supporting Information Fig. S5), but the molecular mechanism underlying the pathogenesis of DACI is complicated and remains unclear, leading to a lack of pharmacologic strategies for

(N) Hippocampal lactate levels of mice in each group were measured using commercial kits ($n = 5$ per group). (O) Representative images and quantification of Nissl staining and $NeuN^+$ cells in DG ($n = 3$ per group). Scale bar, 50 μm. Data are presented as mean ± SEM. *P* values were determined by one-way ANOVA, followed by Turkey's test.

patient management. In this study, upregulated brain endothelial HIF-1α in T2D was found to exacerbate cognitive impairment by accelerating glycolysis-driven lactate production. Brain ECs-specific knockdown of *HIF-1α* resulted in a decrease of hippocampal lactate, thereby enhancing AHN to rescue DACI. Additionally, AA was identified to inhibit HIF-1α-driven lactate production in brain ECs, subsequently ameliorating cognitive dysfunction of T2D mice. Overall, this study highlights the biological significance of brain endothelial HIF-1α-driven lactate in promoting the development of DACI, which suggests that targeting inhibition of HIF-1α in brain ECs represents a potential therapeutic avenue for DACI.

Lactate homeostasis is crucial for maintaining normal brain activity[14,33]; however, the precise biological role of lactate in cognitive impairment remains inconclusive. On one hand, lactate disrupts synaptic plasticity, accelerates β-amyloid aggregation, and promotes microglia polarization, leading to cognitive impairment[36,37]. On the other hand, lactate ameliorates neuronal apoptosis and reduces the inflammatory phenotype of microglia to alleviate memory deficits[38]. Two factors may account for the divergent effects of lactate. Firstly, alterations in lactate levels differ across distinct types of cognitive dysfunction. Numerous studies have consistently shown that CSF lactate levels are significantly elevated in Alzheimer's disease (AD) patients compared to age-matched healthy controls[39−41]. However, recent evidence suggests lactate levels undergo dynamic alteration during the progression of cognitive impairment in AD patients[42,43]. Zebhauser et al.[43] noticed that AD patients at the mild cognitive impairment stage exhibited higher lactate levels than those with dementia, while no significant difference was detected in CSF lactate levels between AD dementia patients and healthy controls. Elevated lactate levels have also been observed in the CSF of vascular dementia (VaD) patients[41] and the hippocampus of VaD rats[44]. Notably, serum lactate levels exhibited an opposite trend in AD and VaD mouse models. As shown in Supporting Information Fig. S6, *db/db* mice exhibited a significant increase in serum lactate levels compared with controls, whereas *APP/PS1* mice, β-amyloid-injected mice, and VaD mice showed a remarkable decrease. No significant difference in serum lactate levels was observed between donepezil-induced mice and control group. Secondly, different cells show heterogeneous responses to changes in lactate levels. For example, neurons uptake lactate as an energy substrate to maintain normal physiological functions. However, elevated hippocampal lactate directly stimulates the H3K18la/NF-κB axis, thereby accelerating microglial cellular senescence[45]. Previous studies have also highlighted that lactate upregulation in astrocytes, driven by enhanced glycolysis, disrupts synaptic plasticity, accelerates β-amyloid aggregation *via* AKT/mTOR/HIF-1α pathway, and consequently leads to spatial cognitive impairment[36]. Here, our results demonstrated a significant association between elevated lactate levels and cognitive impairment in both patients and animal models with T2D. Specifically, our findings provided support for the detrimental impact of hippocampal lactate on AHN under T2D conditions.

AA, a natural triterpenoid compound, exhibits neuroprotective effects in multiple neurological injury disorders[46−48]. Previous studies have demonstrated that treatment with AA reduces apoptosis and promotes axon regeneration of β-amyloid-induced hippocampal neurons *in vitro*, as well as improves cognitive dysfunction *in vivo*[49,50]. Clinical trial results have also confirmed the safety and efficacy of AA[51,52]. Similarly, our findings indicated that AA rescued the memory deficit of DACI mice. Interestingly, despite its strong efficacy, the mechanism underlying the memory-enhancing effects of AA remains poorly investigated. This may be associated with limited BBB permeability for AA[53], as LC−MS analysis revealed that no detectable levels at designated time points (30 and 40 min) during absorption, distribution, and elimination phases[54] following oral administration of AA in both *db/m* and *db/db* mice (Fig. S4). Mechanistic studies on these drugs with low BBB permeability are frequently overlooked by researchers, which impede the identification of potential therapeutic targets for numerous central nervous system (CNS) disorders. In this study, we noted targeted inhibition of HIF-1α expression in brain ECs by AA improved the memory deficit of DACI mice. Therefore, elucidating the mechanism underlying these effective drugs exhibiting low BBB permeability will facilitate identifying potential therapeutic targets.

The BBB, composed of brain ECs, astrocytes, pericytes, and microglia, functions as a protective interface that prevents harmful substances from entering the brain *via* the bloodstream[55]. Structurally, brain ECs constitute the outermost layer of the BBB and are directly exposed to circulating harmful substances[56]. Functionally, they regulate neighboring cells *via* controlled secretion of small molecules, cytokines, and microvesicles that mediate transcellular signaling[57]. Previous studies have demonstrated that R-spondin3 derived from brain ECs can ameliorate ischemic neuronal injury induced by middle cerebral artery occlusion[58]. Moreover, release of microvesicles containing Ascl1 neurotrophic factor by brain ECs induces transdifferentiation of astrocytes into neuroprogenitor cells in a stroke mouse model[59]. In this study, our findings revealed that brain endothelial HIF-1α-driven lactate production exacerbated DACI through inhibiting the proliferation of NSCs. Furthermore, we observed that lactate secreted by brain ECs may impair synaptic function of neurons, reduce astrocytic glutamate uptake, and promote neuroinflammation, thereby amplifying the pathological effects associated with DACI (Supporting Information Fig. S7A−S7C). Consequently, drug intervention strategies targeting brain ECs represent a novel approach for the treatment of CNS diseases.

It is worth mentioning that several limitations still existed here. In Fig. 2A and Fig. S2B, the quantity and average expression of *Hif1a* of microglia were also remarkably increased in *db/db* mice, indicating its underlying biological significance in the pathogenesis of DACI. Previous studies have documented the molecular role of HIF-1α in microglia concerning neuroinflammation[60,61]. For instance, upregulated HIF-1α in microglia triggers an initial phase of acute inflammation followed by a transition into a chronic tolerance state characterized by diminished phagocytic activity[61]. Thus, further evidence is required to determine the potential function of HIF-1α in microglia on neuroinflammation in DACI. Moreover, the molecular mechanism by which elevated hippocampal lactate impairs AHN in DACI remains unclear. AHN is regulated by various classical intracellular signaling pathways and extracellular mediators[62]. A recent study demonstrated that monocarboxylate transporter protein 2 regulates lactate influx in NSCs, thereby promoting H4K12 lactylation, which in turn modulates the MDM2−p53 signaling pathway to influence NSCs proliferation[63]. Another research reported that elevated hippocampal lactate inhibits brain-derived neurotrophic factor transcription *via* a GPR81-dependent mechanism[64]. Our findings demonstrated that brain endothelial HIF-1α-driven lactate production suppressed the proliferation of NSCs, which is

associated with the inhibition of the Wnt/β-Catenin signaling pathway (Supporting Information Fig. S8). Moreover, neurons, astrocytes, and microglia co-cultured with AGEs-induced bEnd.3 cells exhibited signs of functional impairment (Supporting Information Fig. S7). Our results also indicated that AA combined with 2-ME2 could more effectively promote the proliferation of NSCs cocultured with bEnd.3 cells (Supporting Information Fig. S9). Additional experiments are required to further validate these findings and investigate the effects of lactate on other neurogenic or inflammatory pathways that may influence NSCs' proliferation.

5. Conclusions

Taken together, this study first clarifies the biological role of brain endothelial HIF-1α-driven lactate in exacerbating T2D-associated cognitive dysfunction through impairing adult hippocampal neurogenesis. Targeted inhibition of HIF-1α expression in brain ECs through gene editing and pharmacological intervention effectively alleviates DACI, thereby offering novel insights and significant contributions to the comprehension and management of DACI.

Acknowledgements

This study was supported by State Key Laboratory of Bioactive Molecules and Draggability Assessment, Jinan University (No. SKLBMDA-2024109, China), TCM Science and Technology Development Plan of Jiangsu Province (No. ZD202418, China) and Qing Lan Project of Jiangsu Higher Education Institutions (China). We gratefully acknowledge Professor Pan Xiaodong for providing the human samples.

Author contributions

Jicong Chen: Conceptualization; Methodology; Investigation; Visualization; Writing-original draft. Ruohui Lin: Conceptualization; Writing-review & editing. Cuihua Jiang: Methodology. Fang Chen: Investigation; Methodology. Wei Li: Methodology. Lei Wang: Investigation. Ke Pan: Conceptualization; Visualization. Jian Zhang: Investigation. Zhiqi Yin: Conceptualization; Investigation; Writing-review & editing. Yaping Huang: Visualization; Supervision.

Conflicts of interest

The authors declare no conflicts of interest.

Appendix A. Supporting information

Supporting information to this article can be found online at https://doi.org/10.1016/j.apsb.2025.09.028.

References

1. Ciudin A, Espinosa A, Simó-Servat O, Ruiz A, Alegret M, Hernández C, et al. Type 2 diabetes is an independent risk factor for dementia conversion in patients with mild cognitive impairment. *J Diabet Complicat* 2017;**31**:1272−4.
2. Geijselaers SLC, Sep SJS, Stehouwer CDA, Biessels GJ. Glucose regulation, cognition, and brain MRI in type 2 diabetes: a systematic review. *Lancet Diabetes Endocrinol* 2015;**3**:75−89.
3. Miller V, Jenkins DA, Dehghan M, Srichaikul K, Rangarajan S, Mente A, et al. Associations of the glycaemic index and the glycaemic load with risk of type 2 diabetes in 127 594 people from 20 countries (PURE): a prospective cohort study. *Lancet Diabetes Endocrinol* 2024;**12**:330−8.
4. Sloten TT, Sedaghat S, Carnethon MR, Launer LJ, Stehouwer CDA. Cerebral microvascular complications of type 2 diabetes: stroke, cognitive dysfunction, and depression. *Lancet Diabetes Endocrinol* 2020;**8**:325−36.
5. Choudhry H, Harris AL. Advances in hypoxia-inducible factor biology. *Cell Metab* 2018;**27**:281−98.
6. Gunton JE. Hypoxia-inducible factors and diabetes. *J Clin Investig* 2020;**130**:5063−73.
7. Rong J, Han C, Huang Y, Wang Y, Qiu Q, Wang M, et al. Inhibition of xanthine oxidase alleviated pancreatic necrosis *via* HIF-1α-regulated LDHA and NLRP3 signaling pathway in acute pancreatitis. *Acta Pharm Sin B* 2024;**14**:3591−604.
8. Catrina SB, Zheng X. Hypoxia and hypoxia-inducible factors in diabetes and its complications. *Diabetologia* 2021;**64**:709−16.
9. Lei L, Feng J, Wu G, Wei Z, Wang JZ, Zhang B, et al. HIF-1α causes LCMT1/PP2A deficiency and mediates Tau hyperphosphorylation and cognitive dysfunction during chronic hypoxia. *Int J Mol Sci* 2022;**23**: 16140.
10. Li G, Liu J, Guo M, Gu Y, Guan Y, Shao Q, et al. Chronic hypoxia leads to cognitive impairment by promoting HIF-2α-mediated ceramide catabolism and alpha-synuclein hyperphosphorylation. *Cell Death Discov* 2022;**8**:473.
11. Hai Y, Ren K, Zhang Y, Yang L, Cao H, Yuan X, et al. HIF-1α serves as a co-linker between AD and T2DM. *Biomed Pharmacother* 2024; **171**:116158.
12. Li YD, Luo YJ, Xie L, Tart DS, Sheehy RN, Zhang L, et al. Activation of hypothalamic-enhanced adult-born neurons restores cognitive and affective function in Alzheimer's disease. *Cell Stem Cell* 2023;**30**: 415−32.
13. Díaz-Moreno M, Armenteros T, Gradari S, Hortigüela R, García-Corzo L, Fontán-Lozano Á, et al. Noggin rescues age-related stem cell loss in the brain of senescent mice with neurodegenerative pathology. *Proc Natl Acad Sci U S A* 2018;**115**:11625−30.
14. Wang J, Cui Y, Yu Z, Wang W, Cheng X, Ji W, et al. Brain endothelial cells maintain lactate homeostasis and control adult hippocampal neurogenesis. *Cell Stem Cell* 2019;**25**:754−67.
15. Tobin MK, Musaraca K, Disouky A, Shetti A, Bheri A, Honer WG, et al. Human hippocampal neurogenesis persists in aged adults and Alzheimer's disease patients. *Cell Stem Cell* 2019;**24**:974−82.
16. Hayashi K, Kurioka S, Yamaguchi T, Morita M, Kanazawa I, Takase H, et al. Association of cognitive dysfunction with hippocampal atrophy in elderly Japanese people with type 2 diabetes. *Diabetes Res Clin Pract* 2011;**94**:180−5.
17. Stranahan AM, Arumugam TV, Cutler RG, Lee K, Egan JM, Mattson MP. Diabetes impairs hippocampal function through glucocorticoid-mediated effects on new and mature neurons. *Nat Neurosci* 2008;**11**:309−17.
18. Yao Y, Shi J, Zhang C, Gao W, Huang N, Liu Y, et al. Pyruvate dehydrogenase kinase 1 protects against neuronal injury and memory loss in mouse models of diabetes. *Cell Death Dis* 2023;**14**:722.
19. Hussaini SM, Choi CI, Cho CH, Kim HJ, Jun H, Jang MH. Wnt signaling in neuropsychiatric disorders: ties with adult hippocampal neurogenesis and behavior. *Neurosci Biobehav Rev* 2014;**47**:369−83.
20. Wang K, Liu XY, Liu SF, Wang XX, Wei YH, Zhu JR, et al. Rbm24/Notch1 signaling regulates adult neurogenesis in the subventricular zone and mediates Parkinson-associated olfactory dysfunction. *Theranostics* 2024;**14**:4499−518.
21. Zhang J, Rong P, Zhang L, He H, Zhou T, Fan Y, et al. IL4-driven microglia modulate stress resilience through BDNF-dependent neurogenesis. *Sci Adv* 2021;**7**:eabb9888.
22. Jiang W, Zhu F, Xu H, Xu L, Li H, Yang X, et al. CHI3L1 signaling impairs hippocampal neurogenesis and cognitive function in autoimmune-mediated neuroinflammation. *Sci Adv* 2023;**9**:eadg8148.

23. Li Y, Wu L, Yu M, Yang F, Wu B, Lu S, et al. HIF-1α is critical for the activation of Notch signaling in neurogenesis during acute epilepsy. *Neuroscience* 2018;**394**:206−19.
24. Lin CY, Hung SY, Chen HT, Tsou HK, Fong YC, Wang SW, et al. Brain-derived neurotrophic factor increases vascular endothelial growth factor expression and enhances angiogenesis in human chondrosarcoma cells. *Biochem Pharmacol* 2014;**91**:522−33.
25. Madai S, Kilic P, Schmidt RM, Bas-Orth C, Korff T, Büttner M, et al. Activation of the hypoxia-inducible factor pathway protects against acute ischemic stroke by reprogramming central carbon metabolism. *Theranostics* 2024;**14**:2856−80.
26. Liu Z, Dai X, Zhang H, Shi R, Hui Y, Jin X, et al. Gut microbiota mediates intermittent-fasting alleviation of diabetes-induced cognitive impairment. *Nat Commun* 2020;**11**:855.
27. Shi YS, Chen JC, Lin L, Cheng YZ, Zhao Y, Zhang Y, et al. Dendrobine rescues cognitive dysfunction in diabetic encephalopathy by inhibiting ferroptosis *via* activating Nrf2/GPX4 axis. *Phytomedicine* 2023;**119**:154993.
28. Ma S, Bi W, Liu X, Li S, Qiu Y, Huang C, et al. Single-cell sequencing analysis of the *db/db* mouse hippocampus reveals cell-type-specific insights into the pathobiology of diabetes-associated cognitive dysfunction. *Front Endocrinol* 2022;**13**:891039.
29. Xiao H, Zhang M, Xu J, Deng Y, Li N, Gao P, et al. Icarisid II promotes proliferation and neuronal differentiation of neural stem cells *via* activating Wnt/β-catenin signaling pathway. *Phytother Res* 2021; **35**:2773−84.
30. Nicolicht-Amorim P, Delgado-Garcia LM, Nakamura TKE, Courbassier NR, Mosini AC, Porcionatto MA. Simple and efficient protocol to isolate and culture brain microvascular endothelial cells from newborn mice. *Front Cell Neurosci* 2022;**16**:949412.
31. Zhang X, Chen J, Lin R, Huang Y, Wang Z, Xu S, et al. Lactate drives epithelial-mesenchymal transition in diabetic kidney disease *via* the H3K14la/KLF5 pathway. *Redox Biol* 2024;**75**:103246.
32. Xiao HH, Chen JC, Li H, Li RH, Wang HB, Song HP, et al. Icarisid II rescues cognitive dysfunction *via* activation of Wnt/β-catenin signaling pathway promoting hippocampal neurogenesis in APP/PS1 transgenic mice. *Phytother Res* 2022;**36**:2095−108.
33. Li X, Yang Y, Zhang B, Lin X, Fu X, An Y, et al. Lactate metabolism in human health and disease. *Signal Transduct Targeted Ther* 2022;**7**: 305.
34. Feng T, Zhao X, Gu P, Yang W, Wang C, Guo Q, et al. Adipocyte-derived lactate is a signaling metabolite that potentiates adipose macrophage inflammation *via* targeting PHD2. *Nat Commun* 2022;**13**: 5208.
35. Yang K, Fan M, Wang X, Xu J, Wang Y, Gill PS, et al. Lactate induces vascular permeability *via* disruption of VE-cadherin in endothelial cells during sepsis. *Sci Adv* 2022;**8**:eabm8965.
36. Yang X, Chen YH, Liu L, Gu Z, You Y, Hao JR, et al. Regulation of glycolysis-derived L-lactate production in astrocytes rescues the memory deficits and Aβ burden in early Alzheimer's disease models. *Pharmacol Res* 2024;**208**:107357.
37. Zheng X, Hu F, Chen X, Yang G, Li M, Peng Y, et al. Role of microglia polarization induced by glucose metabolism disorder in the cognitive impairment of mice from PM2.5 exposure. *Sci Total Environ* 2024;**954**:176603.
38. Han H, Zhao Y, Du J, Wang S, Yang X, Li W, et al. Exercise improves cognitive dysfunction and neuroinflammation in mice through Histone H3 lactylation in microglia. *Immun Ageing* 2023;**20**:63.
39. Zebhauser PT, Berthele A, Goldhardt O, Diehl-Schmid J, Priller J, Ortner M, et al. Cerebrospinal fluid lactate levels along the Alzheimer's disease continuum and associations with blood−brain barrier integrity, age, cognition, and biomarkers. *Alzheimers Res Ther* 2022; **14**:61.
40. Liguori C, Chiaravalloti A, Sancesario G, Stefani A, Sancesario GM, Mercuri NB, et al. Cerebrospinal fluid lactate levels and brain [^{18}F] FDG PET hypometabolism within the default mode network in Alzheimer's disease. *Eur J Nucl Med Mol Imag* 2016;**43**:2040−9.
41. Parnetti L, Reboldi GP, Gallai V. Cerebrospinal fluid pyruvate levels in Alzheimer's disease and vascular dementia. *Neurology* 2000;**54**: 735−7.
42. Liguori C, Stefani A, Sancesario G, Sancesario GM, Marciani MG, Pierantozzi M. CSF lactate levels, τ proteins, cognitive decline: a dynamic relationship in Alzheimer's disease. *J Neurol Neurosurg Psychiatry* 2015;**86**:655−9.
43. Zebhauser PT, Berthele A, Goldhardt O, Diehl-Schmid J, Priller J, Ortner M, et al. Cerebrospinal fluid lactate levels along the Alzheimer's disease continuum and associations with blood-brain barrier integrity, age, cognition, and biomarkers. *Alzheimers Res Ther* 2022; **14**:61.
44. Sun W, Chen YH, Song YY, Wu T, Zhao HX, Wang HY, et al. Electroacupuncture improves cognitive function by modulating hippocampal lactate-mediated HIF-1α signaling pathway and inhibiting inflammation response in vascular dementia rats. *Acupunct Res* 2024; **49**:1010−8.
45. Wei L, Yang X, Wang J, Wang Z, Wang Q, Ding Y, et al. H3K18 lactylation of senescent microglia potentiates brain aging and Alzheimer's disease through the NFκB signaling pathway. *J Neuroinflammation* 2023;**20**:208.
46. He Z, Hu Y, Niu Z, Zhong K, Liu T, Yang M, et al. A review of pharmacokinetic and pharmacological properties of asiaticoside, a major active constituent of *Centella asiatica* (L.) Urb. *J Ethnopharmacol* 2023;**302**:115865.
47. Bandopadhyay S, Mandal S, Ghorai M, Jha NK, Kumar M, null Radha, et al. Therapeutic properties and pharmacological activities of asiaticoside and madecassoside: a review. *J Cell Mol Med* 2023;**27**:593−608.
48. Park JH, Seo YH, Jang JH, Jeong CH, Lee S, Park B. Asiatic acid attenuates methamphetamine-induced neuroinflammation and neurotoxicity through blocking of NF-κB/STAT3/ERK and mitochondria-mediated apoptosis pathway. *J Neuroinflammation* 2017;**14**:240.
49. Halder T, Patel B, Acharya N. Asiatic acid fabricated nanoconstructs to mitigate amyloid beta1-42 induced injury in SH-SY5Y Cells *in-vitro* and ameliorates cognitive impairment by dual cholinesterase inhibition and attenuation of oxidative stress *in-vivo*. *Pharm Res* 2023; **40**:197−213.
50. Hannan MA, Haque MN, Munni YA, Oktaviani DF, Timalsina B, Dash R, et al. *Centella asiatica* promotes early differentiation, axodendritic maturation and synaptic formation in primary hippocampal neurons. *Neurochem Int* 2021;**144**:104957.
51. Lou JS, Dimitrova DM, Murchison C, Arnold GC, Belding H, Seifer N, et al. *Centella asiatica* triterpenes for diabetic neuropathy: a randomized, double-blind, placebo-controlled, pilot clinical study. *Esper Dermatol* 2018;**20**:12−22.
52. Songvut P, Chariyavilaskul P, Tantisira MH, Khemawoot P. Safety and pharmacokinetics of standardized extract of centella asiatica (ECa 233) capsules in healthy thai volunteers: a phase 1 clinical study. *Planta Med* 2019;**85**:483−90.
53. Raval N, Barai P, Acharya N, Acharya S. Fabrication of peptide-linked albumin nanoconstructs for receptor-mediated delivery of asiatic acid to the brain as a preventive measure in cognitive impairment: optimization, *in-vitro* and *in-vivo* evaluation. *Artif Cells, Nanomed Biotechnol* 2018;**46**:S832−46.
54. Yuan Y, Zhang H, Sun F, Sun S, Zhu Z, Chai Y. Biopharmaceutical and pharmacokinetic characterization of asiatic acid in *Centella asiatica* as determined by a sensitive and robust HPLC−MS method. *J Ethnopharmacol* 2015;**163**:31−8.
55. Cunha S, Bicker J, Sereno J, Falcão A, Fortuna A. Blood brain barrier dysfunction in healthy aging and dementia: why, how, what for?. *Ageing Res Rev* 2024;**99**:102395.
56. Hang Z, Zhou L, Xing C, Wen Y, Du H. The blood−brain barrier, a key bridge to treat neurodegenerative diseases. *Ageing Res Rev* 2023; **91**:102070.
57. Díaz-Castro B, Robel S, Mishra A. Astrocyte endfeet in brain function and pathology: open questions. *Annu Rev Neurosci* 2023;**46**:101−21.

58. Shimamura M, Hayashi H, Ju N, Yoshida S, Baba S, Sasaki T, et al. *R*-Spondin 3/LGR4 (leucine-rich repeat-containing G protein-coupled receptor 4) axis is a novel inflammatory and neurite outgrowth signaling system in the ischemic brain in mice. *Stroke* 2023;**54**: 1606−15.
59. Li W, Mandeville ET, Durán-Laforet V, Fukuda N, Yu Z, Zheng Y, et al. Endothelial cells regulate astrocyte to neural progenitor cell trans-differentiation in a mouse model of stroke. *Nat Commun* 2022; **13**:7812.
60. Gedam M, Comerota MM, Propson NE, Chen T, Jin F, Wang MC, et al. Complement C3aR depletion reverses HIF-1α-induced metabolic impairment and enhances microglial response to Aβ pathology. *J Clin Investig* 2023;**133**:e167501.
61. Baik SH, Kang S, Lee W, Choi H, Chung S, Kim JI, et al. A breakdown in metabolic reprogramming causes microglia dysfunction in Alzheimer's disease. *Cell Metab* 2019;**30**:493−507.
62. Tang C, Wang Q, Shen J, Wang C, Ding H, Wen S, et al. Neuron stem cell NLRP6 sustains hippocampal neurogenesis to resist stress-induced depression. *Acta Pharm Sin B* 2023;**13**:2017−38.
63. Li Z, Liang Z, Qi H, Luo X, Wang M, Du Z, et al. Lactate shuttling links histone lactylation to adult hippocampal neurogenesis in mice. *Dev Cell* 2025;**60**:1182−98.
64. Zhao L, Dong M, Ren M, Li C, Zheng H, Gao H. Metabolomic analysis identifies lactate as an important pathogenic factor in diabetes-associated cognitive decline rats. *Mol Cell Proteomics* 2018; **17**:2335−46.